INORGANIC CHEMISTRY
FRONTIERS

RESEARCH ARTICLE

View Article Online
View Journal | View Issue

Cite this: *Inorg. Chem. Front.*, 2020, **7**, 4077

Controllable synthesis of hierarchical Au/PdAg heterostructures consisting of nanosheets on nanorods with plasmon-enhanced electrocatalytic properties†

Zhiqiang Ge,‡ Cheng Wang‡ and Limin Qi *

Received 6th August 2020,
Accepted 9th September 2020

DOI: 10.1039/d0qi00945h

rsc.li/frontiers-inorganic

Hierarchical hybrid metal nanostructures with complex architectures are attracting considerable attention because of their tunable properties, novel functions, and promising applications. In this work, the controllable synthesis of unique hierarchical Au/PdAg heterostructures consisting of regularly aligned PdAg nanosheets epitaxially grown on Au nanorods (Au/PdAg NRNSs) was realized in the presence of a mixture of dodecyltrimethylammonium bromide (DTAB) and cetyltrimethylammonium bromide (CTAB). If DTAB was used as the single surfactant, PdAg nanodendrite-tipped Au nanorods (Au/PdAg NRNDs) were produced, whereas Pd nanoblock-tipped Au nanorods (Au/Pd NRNBs) were obtained in the absence of Ag^+ ions. It was revealed that a desirable combination of appropriate DTAB and CTAB concentrations is crucial to the formation of the unusual Au/PdAg NRNSs. When the three nano-heterostructures were used as catalysts for the electrocatalytic hydrogen evolution reaction, the Au–PdAg NRNSs exhibited the best catalytic performance. Furthermore, all of the three heterostructures showed pronounced plasmon-enhanced electrocatalytic activity with the Au/PdAg NRNSs exhibiting the best photo-assisted electrocatalytic activity. This work may open new avenues toward rational design and controllable synthesis of well-defined heterostructured nanoparticles with novel architectures and promising applications.

Introduction

Heterostructured nanoparticles are a typical kind of hybrid nanostructure comprising two or more distinctive nanoscale components. Owing to the combination of two different components, tunable properties, superior performance, and novel functions or applications may arise from the cooperative and synergistic effects.[1–3] Considering that the properties of hybrid nanostructures are largely dependent on the composition and structure of each component as well as the three-dimensional (3D) architecture of the heterostructures, significant efforts have been devoted to the rational design and controllable synthesis of hybrid nanostructures with complex 3D architectures. It is notable that epitaxial growth has been demonstrated to be a promising approach toward elaborate hybrid nanostructures with well-defined 3D architectures.[4,5] Particularly, epitaxial growth of one-dimensional (1D) nanorods or nanowires and two-dimensional (2D) nanosheets or nanoplates on 1D nanowires leads to well-defined branched nanowires, which represent hierarchical 1D–1D and 2D–1D heterostructures, respectively. For example, Zhang and co-workers reported the fabrication of 1D–1D heterostructures through epitaxial growth of Ru nanorods on crystal-phase heterostructured 4H/fcc Au nanowires,[6] and the preparation of 2D–1D heterostructures *via* epitaxial growth of MoS_2 or $MoSe_2$ nanosheets along the backbones of $Cu_{2-x}S$ nanowires.[7] However, it remains challenging to develop feasible epitaxial growth methods to realize the controlled synthesis of hierarchical heterostructures with desired compositions and architectures.

Among various heterostructured nanoparticles, hybrid noble metal nanocrystals have attracted considerable attention because of their unique optical, electrical, and chemical properties associated with noble metals.[8–10] On the one hand, noble metals including Au and Ag show size- and shape-dependent optical properties and fascinating surface plasmonic resonance (SPR) characteristics. In this regard, tremendous efforts have been devoted to the shape-controlled synthesis of gold nanocrystals and the exploration of their shape-dependent properties.[11–14] It is noteworthy that plasmon-mediated catalysis, which includes plasmon-driven and plasmon-enhanced processes, has stimulated intense interest in various catalytic reactions involving plasmonic nanoparticles.[15–18] On

Beijing National Laboratory for Molecular Sciences (BNLMS), College of Chemistry, Peking University, Beijing 100871, China. E-mail: liminqi@pku.edu.cn

†Electronic supplementary information (ESI) available: Additional TEM characterizations. See DOI: 10.1039/d0qi00945h

‡These two authors contributed equally.

the other hand, noble metals such as Pt and Pd exhibit excellent catalytic activity and have been widely used in a variety of heterogeneous catalysis and electrocatalysis processes. Notably, the catalytic activity of noble metal nanoparticles largely depends on their size and morphology.[19,20] Furthermore, noble metal alloy (*e.g.*, PdAg alloy) nanoparticles can exhibit enhanced catalytic performance compared with single-component noble metal (*e.g.*, Pd) nanoparticles because of favorable electronic, surface, and morphological modulations.[21–24] The hybridization of plasmonic noble metal nanoparticles with catalytically active noble metal nanoparticles would endow the nano-heterostructures with improved catalytic performance under light illumination because of plasmon-enhanced catalysis, where the hot electron transfer, photothermal effect, and local electromagnetic field enhancement are believed to play key roles.[10,16–18] Therefore, the rational design and synthesis of hybrid noble metal nanoparticles with significant plasmon-enhanced catalytic properties have become an appealing approach.

As typical anisotropic metal nanocrystals exhibit remarkable SPR properties, gold nanorods (Au NRs or GNRs) have received tremendous attention.[25] A variety of Au–Pd nanoheterostructures based on GNRs have been fabricated through controlled growth on the GNRs. For example, Au@Pd core–shell nanorods were readily synthesized, and both the growth mechanism[26] and the light-driven catalytic organic synthesis[27] were investigated. Interestingly, Au–Pd supra-nanoparticles consisting of densely packed anisotropic Pd nanostructures surrounding GNRs were prepared instead of core–shell nanorods when the GNRs were modified with a mixture of cetyltrimethylammonium bromide (CTAB) and 5-bromosalicylic acid.[28] It is noteworthy that there are several reports on the synthesis and plasmon-enhanced catalysis of hierarchical Au–Pd heterostructures made of GNRs covered by 1D Pd nanostructures; examples include Au–Pd superstructures with ordered Pd nanoarrays precisely grown on GNRs for plasmon-enhanced carbon–carbon coupling reactions,[29] Pd nanodendrite-tipped GNRs for plasmon-enhanced Suzuki cross-coupling reactions,[30] and Pd-tipped GNRs for plasmon-enhanced electrocatalytic hydrogen evolution.[31] Furthermore, Au@PdAg core–shell nanorods were obtained from conversion of Au@Pd core–shell nanorods.[32] Some hierarchical Au–PdAg heterostructures based on GNRs were synthesized through CTAB-assisted overgrowth on GNRs[33] and conversion of Au@Ag core–shell nanorods,[34,35] and their applications in electrocatalytic ethanol oxidation were explored. Despite considerable progress in the preparation of Au–Pd or Au–PdAg heterostructures, it remains a challenge to controllably synthesize epitaxial heterostructures with well-defined and novel architectures.

In this work, the controlled synthesis of unique hierarchical Au/PdAg heterostructures consisting of regularly aligned PdAg nanosheets grown perpendicularly on Au nanorods (Au/PdAg NRNSs) was realized, which may represent the first example of epitaxial 2D–1D hybrid noble metal nanostructures. The epitaxial growth of arrayed PdAg nanosheets on the four lateral {100} facets of the [100]-oriented GNRs was achieved in aqueous solution with the assistance of a mixture of dodecyltrimethylammonium bromide (DTAB) and CTAB. In contrast, without addition of CTAB, PdAg nanodendrite-tipped Au nanorods (Au/PdAg NRNDs) were produced, whereas Pd nanoblock-tipped Au nanorods (Au/Pd NRNBs) were obtained in the absence of Ag^+ ions. When the three nano-heterostructures were used as catalysts for the electrocatalytic hydrogen evolution reaction (HER), the Au–PdAg NRNSs exhibited the best catalytic performance; furthermore, all of the three heterostructures showed pronounced plasmon-enhanced catalytic activity.

Experimental section

Chemicals

Dodecyltrimethylammonium bromide (DTAB, 99%) and cetyltrimethylammonium bromide (CTAB, 99%) were purchased from Sigma. Silver nitrate ($AgNO_3$, 99.8%) and hydrochloroauric acid trihydrate ($HAuCl_4{\cdot}3H_2O$, 99.9%) were obtained from Beijing Chemical Reagents Co. Palladium(II) chloride ($PdCl_2$) was from Beijing Tongguang Chemical Co. Sodium borohydride was purchased from Guoyao Chemical Co., and hydroquinone and ascorbic acid (>99.7%) were obtained from Xilong chemical Co. All aqueous solutions were prepared from ultra-pure water.

Synthesis of gold nanorods (Au NRs)

The synthesis of Au NRs (*i.e.*, GNRs) was carried out using a seed-mediated method following the reported method[36] with minor modification. For the preparation of a seed solution, 0.5 mL of 10 mM $HAuCl_4$ solution was added into 10 mL of 0.1 M CTAB solution in a glass vessel. A solution of 0.01 M sodium borohydride dissolved in 0.01 M sodium hydroxide was freshly prepared. Then, 0.6 mL of 10 mM sodium borohydride solution was injected into the mixture under vigorous stirring. After 10 s of stirring, the resultant seed solution was aged for 30 min at 30 °C before use. For the preparation of a growth solution, 200 mL of 100 mM CTAB solution was mixed with 10 mL of 10 mM $HAuCl_4$ solution and 8 mL of 10 mM $AgNO_3$ solution. Then, 10 mL of 100 mM hydroquinone solution was added, which was followed by vigorous stirring for 1 min. Finally, the growth of GNRs was triggered by adding 1.6 mL of the seed solution into the growth solution. The reaction mixture was left undisturbed overnight at 30 °C. The resultant GNR dispersion was centrifuged, and the GNRs were redispersed in 1 mM CTAB solution to form a 10-fold concentrated GNR dispersion as a GNR seed solution for further overgrowth.

Synthesis of gold nanorods tipped by Pd nanoblocks (Au/Pd NRNBs)

A 10 mM H_2PdCl_4 solution was first prepared by dissolving $PdCl_2$ (44.6 mg) in 25 mL of HCl solution (pH = 1.69). Then, 9.2 mL of water was mixed with 0.3 mL of 3 mM DTAB solu-

tion, 0.1 mL of 10 mM H_2PdCl_4 solution, and 0.2 mL of the GNR seed solution. Then, 0.2 mL of 100 mM ascorbic acid was quickly injected into the mixture under stirring. Finally, the solution mixture was left undisturbed at 30 °C for 12 h in a water bath. The resultant Au/Pd NRNBs were washed twice with water by centrifugation at 5400 rpm for 10 min to remove the extra DTAB.

Synthesis of gold nanorods tipped by PdAg nanodendrites (Au/PdAg NRNDs)

The Au/PdAg NRNDs were synthesized under conditions similar to the synthesis of Au–Pd NRNBs except for the addition of Ag^+ ions. In a typical synthesis, 9.15 mL of water was first mixed with 0.3 mL of 3 mM DTAB solution, 0.1 mL of 10 mM H_2PdCl_4 solution, 0.05 mL of 10 mM $AgNO_3$ solution, and 0.2 mL of the GNR seed solution. Then, 0.2 mL of 100 mM ascorbic acid solution was quickly injected into the mixture under stirring. Finally, the solution mixture was left undisturbed at 30 °C for 12 h in a water bath. The resultant Au/PdAg NRNDs were washed twice with water by centrifugation at 5400 rpm for 10 min to remove the extra DTAB. Additionally, dense Au–PdAg NRNDs were prepared by increasing the H_2PdCl_4 concentration in the solution from 0.1 mM to 0.4 mM while the Pd/Ag molar ratio in the solution was kept at 2 : 1.

Synthesis of gold nanorods attached by PdAg nanosheets (Au/PdAg NRNSs)

The Au/PdAg NRNSs were synthesized under conditions similar to the synthesis of Au–PdAg NRNDs except for the introduction of CTAB. In a typical synthesis, 0.3 mL of 10 mM DTAB solution, 0.1 mL of 10 mM H_2PdCl_4 solution, 0.05 mL of 10 mM $AgNO_3$ solution and 0.2 mL of the GNR seed solution were added to 9.05 mL of water sequentially. Then, the mixture was added to 0.1 mL of 100 mM CTAB solution, and 0.2 mL of 100 mM ascorbic acid solution was added quickly, which followed by 20 s of rigorous stirring. Then, the solution was left undisturbed at 30 °C for 12 h in a water bath. The resultant Au/PdAg NRNSs were washed twice with water by centrifugation at 5400 rpm for 10 min to remove the extra DTAB and CTAB. Additionally, dense Au–PdAg NRNSs were prepared by increasing the H_2PdCl_4 concentration in the solution from 0.1 mM to 0.4 mM while the Pd/Ag molar ratio in the solution was kept at 2 : 1.

Characterization

The Au/Pd and Au/PdAg heterostructures were characterized by scanning electron microscopy (SEM, Hitachi FEI S4800 and FEI Helios G4 UX, 10 kV), transmission electron microscopy (TEM, FEI Tecnai T20, 200 kV), high-resolution TEM (HRTEM, FEI Tecnai F30, 300 kV), and UV-vis-NIR spectroscopy (PerkinElmer Lambda 950).

Electrochemical measurements

For the catalytic electrode modification, an L-type glassy carbon electrode was polished using alumina slurries with 0.3 μm and 0.05 μm in diameter. Then the polished L-type glassy carbon electrode was sonicated three times in water for 30 s each time to remove the residual polishing agent. Subsequently, 10 μL of the treated mixed solution ($V_{water} : V_{ethanol} : V_{5\%\ Nafion\ solution}$ = 4 : 1 : 0.25) was added dropwise to the treated L-type glassy carbon electrode (the total loading of Pd was 0.15 mg cm^{-2}) and dried at room temperature.

All electrochemical measurements were performed at room temperature on a CHI 660C electrochemical workstation (Shanghai Chenhua Instruments Inc.). Polarization curves were obtained by linear sweep voltammetry at a scan rate of 5 mV s^{-1} in 0.5 M H_2SO_4 solution. In all electrochemical tests, the modified glassy carbon electrode and the graphite rod electrode were used as the working electrode and the counter electrode, respectively, while the Ag/AgCl electrode was used as the reference electrode. In the photo-assisted electrocatalytic test, the working electrode was illuminated with a 300 W xenon lamp at a distance of 15 cm. The temperature of the electrocatalytic system was kept constant under dark and light irradiation to eliminate the effects of the temperature change caused by light irradiation on the electrocatalytic activity.

Results and discussion

The GNRs used as seeds for the secondary growth of Pd or PdAg alloy nanostructures were prepared by a seed-mediated procedure using hydroquinone as a reducing agent, which led to high-yield synthesis of [100]-oriented single-crystal gold nanorods with relatively large aspect ratios.[36,37] The SEM image shown in Fig. 1a suggests that the produced GNRs are uniform with an average length of ~93 nm and an average diameter of ~13 nm, giving an aspect ratio of ~7.2, as confirmed by the particle size distribution diagram (Fig. S1†). The related TEM image shows that the GNRs have straight side edge lines

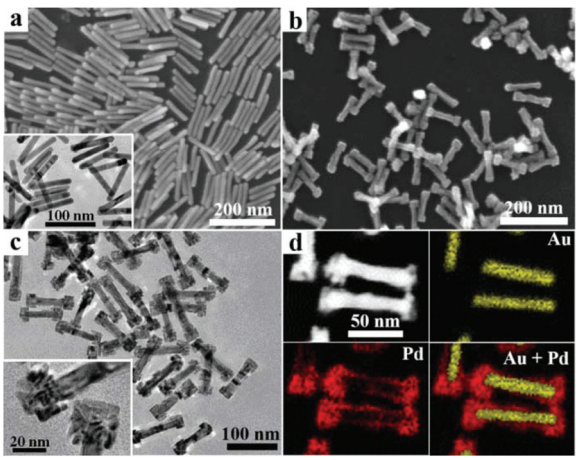

Fig. 1 (a) SEM and TEM (inset) images of Au NRs. SEM (b) and TEM (c) images of Au/Pd NRNBs. The inset shows an enlarged TEM image of the nanoblocks tipped at the ends of Au/Pd NRNBs. (d) HAADF-STEM image of Au/Pd NRNBs and corresponding elemental mapping of Au and Pd.

and relatively sharp tips on both ends. Au/Pd heterostructured nanoparticles were obtained by reducing H_2PdCl_4 with ascorbic acid using the GNRs as seeds in the presence of 0.1 mM H_2PdCl_4 and 3 mM DTAB. As shown in Fig. 1b, uniform Pd nanoblock-tipped Au nanorods (Au/Pd NRNBs) ~105 nm in length were obtained. The TEM images shown in Fig. 1c suggest that two quasi-cuboidal nanoblocks ~25 nm in width are tipped on both ends while the central part of the nanorods is slightly widened to ~15 nm, indicating preferential growth of Pd crystal blocks on the ends and minor Pd deposition on the lateral surfaces. This result is consistent with the elemental analysis by high-angle annular dark-field scanning transmission electron microscopy (HAADF-STEM) shown in Fig. 1d, which reveals that the Pd element is mainly distributed in the nanoblocks tipped on both ends and also present in the thin layer covering the lateral sides of the middle part of the GNRs. The HRTEM image of the nanoblock shows clear lattice fringes with a spacing of 0.22 nm (Fig. S2†), which corresponds to the (111) plane of metallic Pd, confirming that the nanoblocks are essentially Pd single crystals despite the existence of many defects. The preferential growth of Pd on both ends of GNRs could be partially ascribed to the relatively large curvature of the ends, which results in looser packing of the capping DTAB molecules.

If 0.05 mM $AgNO_3$ was added to the growth solution containing 0.1 mM H_2PdCl_4, PdAg alloy nanodendrites instead of Pd nanoblocks were grown on both ends of the GNRs. Uniform dumbbell-shaped heterostructures made of PdAg nanodendrites tipped on both ends of the Au nanorods (Au/PdAg NRNDs) were obtained (Fig. 2a and b). The nanodendrites are composed of loosely aligned anisotropic PdAg nanostructures (Fig. 2c). The elemental mapping result indicates that the Pd and Ag element patterns are very similar, and they are distributed predominantly on both swollen ends of the dumbbells, indicating the formation of the dendrites composed of the PdAg alloy (Fig. 2d). The related energy dispersive X-ray spectroscopy (EDS) analysis suggests that the Pd/Ag molar ratio in the PdAg alloy is ~2.2 : 1, which is somewhat higher than that in the reaction solution (2 : 1), indicating a relatively higher tendency of Pd deposition. The HRTEM image of the nanodendrite shows clear lattice fringes with a spacing of 0.23 nm (Fig. S3†), which is slightly larger than the interplanar spacing (0.22 nm) of the Pd (111) plane, and actually corresponds to the (111) plane of the PdAg alloy. The formation of nanodendrites instead of nanoblocks upon addition of the Ag^+ ion could be attributed to the difference in the crystallization characteristics of the Pd metal and PdAg alloy since hyperbranched PdAg alloy nanoparticles were readily formed in a similar DTAB solution without the seed GNRs.[38] When the concentration of the H_2PdCl_4 was increased from 0.1 mM to 0.4 mM while the Pd/Ag molar ratio in the solution was kept at 2 : 1, dense Au/PdAg NRNDs consisting of GNRs almost fully covered by dense PdAg nanodendrites were obtained (Fig. 2e and f), suggesting that the PdAg alloy nanodendrites preferentially deposited on both ends of the GNRs, and the deposition gradually extended to the middle part of the GNRs with increasing the feeding Pd and Ag amounts, leading to nearly full coverage.

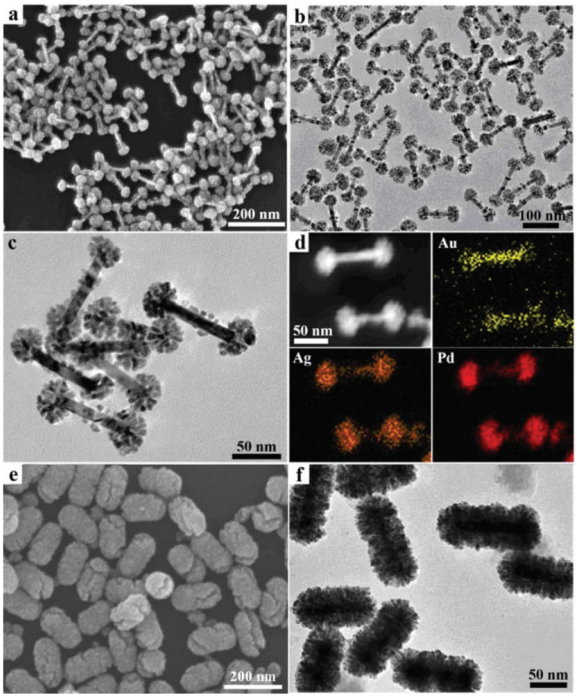

Fig. 2 SEM (a) and TEM (b and c) images of Au/PdAg NRNDs. (d) HAADF-STEM image of Au/PdAg NRNDs and corresponding elemental mapping of Au, Pd and Ag. SEM (e) and TEM (f) images of dense Au/PdAg NRNDs.

Interestingly, the introduction of 1 mM CTAB to the growth solution containing 3 mM DTAB resulted in the formation of unusual hierarchical heterostructures consisting of PdAg alloy nanosheets epitaxially grown on the Au nanorods (Au/PdAg NRNSs), which may represent the first example of 2D–1D hybrid noble metal nanostructures. As shown in Fig. 3a, the Au/PdAg nano-heterostructures obtained in the mixed DTAB/CTAB surfactant system are uniform branched nanorods comprising parallel nanosheets, which are perpendicular to the length axis of the nanorods. The uniform Au/PdAg NRNSs are ~105 nm in length and ~28 nm in diameter (Fig. S4†). Closer observation suggests that there are four distinct grooves between the four well-aligned nanosheet arrays grown on the GNRs in a crisscross manner (Fig. 3b), indicating epitaxial growth of the nanosheets on the four symmetric side facets of the GNRs. The TEM image shown in Fig. 3c confirms that the branched nanorods consist of well-defined nanosheet arrays aligned in parallel showing a 4-fold symmetry with respect to the length axis. The elemental analysis by HAADF-STEM demonstrates that the well-aligned nanosheet arrays are composed of the PdAg alloy. The related EDS analysis suggests that the Pd/Ag molar ratio in the PdAg alloy is ~2.1 : 1. The high-magnification TEM image shown in Fig. 3e suggests that the parallel nanosheets are about 9 nm in width and about 5 nm in thickness; notably, the spacings between two neighboring nanosheets are almost identical. The HRTEM image shows

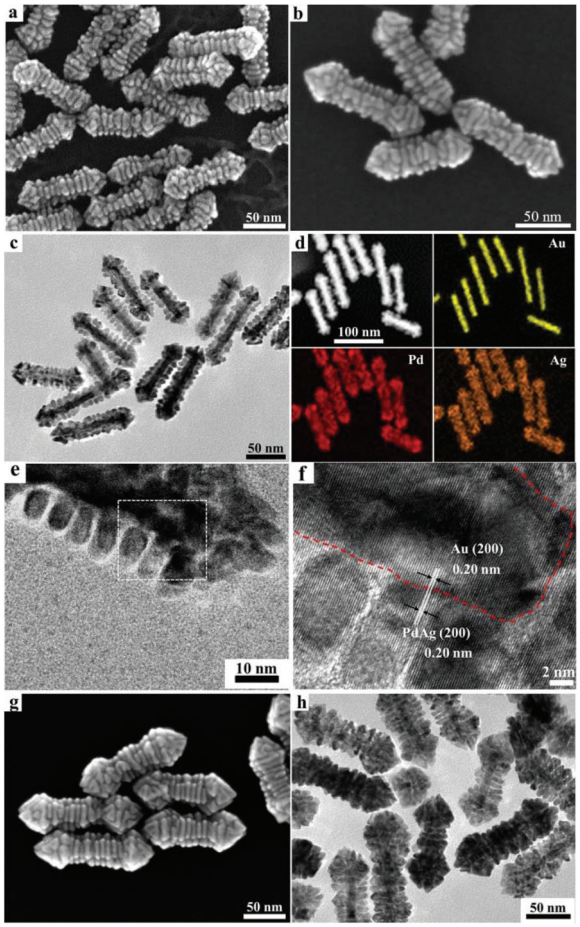

Fig. 3 SEM (a and b) and TEM (c) images of Au/PdAg NRNSs. (d) HAADF-STEM image of Au/PdAg NRNSs and corresponding elemental mapping of Au, Pd and Ag. High-magnification TEM (e) and HRTEM (f) images of Au/PdAg NRNSs. The HRTEM image corresponds to the framed area in panel e. SEM (g) and TEM (h) images of dense Au/PdAg NRNSs.

clear lattice fringes with an interplanar spacing of 0.20 nm throughout the regions of Au nanorods and PdAg alloy nanosheets (Fig. 3f), implying almost perfect lattice matching between the Au (200) plane and the PdAg alloy (200) plane, which is favorable for the epitaxial growth. Such a lattice matching between the Au (200) plane and the PdAg alloy (200) plane can be frequently observed for the Au/PdAg NRNSs even though the boundary between the Au and PdAg alloy is hard to discern (Fig. S5†). This result strongly indicates that the PdAg alloy nanosheets with exposed (100) facets were grown epitaxially on the four lateral {100} facets of the [100]-oriented Au nanorods, leading to the formation of the unique hierarchical Au/PdAg NRNSs showing a 4-fold symmetry. When the concentration of the H_2PdCl_4 was increased from 0.1 mM to 0.4 mM while the Pd/Ag molar ratio in the solution was kept at 2 : 1, dense Au/PdAg NRNSs consisting of GNRs almost fully covered by densely packed PdAg nanosheets were obtained (Fig. 3g and h), suggesting that the PdAg alloy nanosheets became thicker and wider with increasing the feeding Pd and Ag amounts.

To shed light on the formation mechanism of the unusual heterostructured Au/PdAg NRNSs in the mixed DTAB/CTAB surfactant system, we investigated the effects of the concentration of DTAB relative to CTAB in the growth solution on the morphology of the final Au/PdAg hybrid nanostructures through the variation of the CTAB concentration at a fixed DTAB concentration and the variation of DTAB concentration at a fixed CTAB concentration. When the DTAB concentration was kept at 3 mM, GNRs tipped by PdAg nanodendrites were formed at a low CTAB concentration of 0.12 mM; some PdAg nanosheets were grown on the side surfaces of the GNRs when the CTAB concentration was increased to 0.17 mM; the typical Au/PdAg NRNSs were produced at a medium CTAB concentration of 1 mM; the PdAg nanosheets partially fused when the CTAB concentration was increased to 5.0 mM; significant coalescence of the PdAg nanosheets occurred upon further increasing the CTAB concentration to 10 mM (Fig. S6†). Overall, the morphology of the Au/PdAg heterostructures varies from preferential deposition of nanodendrites on both ends of the GNRs through epitaxial growth of nanosheets on the lateral facets of the GNRs to nearly conformal deposition of a thin layer with irregular protrusions on the lateral surfaces with increasing CTAB concentration. This result indicates that a gradual transition from kinetic control to thermodynamic control for the growth mode of PdAg occurred upon increasing the CTAB concentration. On the other hand, the presence of a suitable concentration of DTAB (*e.g.*, 3 mM) is essential to the formation of the well-defined Au/PdAg NRNSs. At a fixed CTAB concentration of 1 mM, particle-tipped nanorods together with irregular particles formed in the absence of DTAB, and the GNRs were covered by partially fused nanosheets at a high DTAB concentration of 10 mM (Fig. S7†).

It has been documented that the morphology of a hybrid metal nanocrystal formed by seed-mediated growth can be determined by the ratio between the deposition rate (V_{dep}) and diffusion rate (V_{diff}) of the secondary metal on the surface of the seed metal.[39] In the current situation, the V_{dep} of PdAg would be decreased with increasing CTAB concentration since the CTAB molecule has a longer alkyl chain compared with DTAB, which would lead to a stronger capping on the surface of GNRs as well as a stronger bonding between the CTA^+ ions and the $PdCl_4^{2-}$ ions in the solution. At a low CTAB concentration coupled with 3 mM DTAB, the V_{dep} is considerably larger than the V_{diff} and the "hit-and-stick" growth mode is dominant, leading to the formation of nanodendrite-tipped nanorods; at a medium CTAB concentration, the V_{dep} is comparable to the V_{diff}, resulting in the epitaxial growth of PdAg nanosheets on the GNRs; at a high CTAB concentration, the V_{dep} is considerably lower than the V_{diff} and the "hit-and-run" growth mode is dominant, leading to the nearly conformal deposition of a PdAg thin layer. On the other hand, in the 1 mM CTAB solution without DTAB, the preferential deposition on the ends also occurred, which was accompanied by the direct precipitation of PdAg particles in solution because the CTAB-capped GNRs are not favorable for the heterogeneous deposition of PdAg; when a high concentration of

DTAB was coupled with 1 mM CTAB, the V_{dep} of PdAg was also considerably lowered, leading to the partial fusion of the PdAg nanosheets. Therefore, a desirable combination of appropriate DTAB and CTAB concentrations is crucial to the formation of the unique Au/PdAg NRNSs.

Based on these observations, a tentative growth mechanism of the three different nano-heterostructures is proposed as follows (Fig. 4): in the presence of 3 mM DTAB, preferential deposition of Pd nanoblocks on both ends of the DTAB-capped GNRs occurs because the molecular chains of CTAB at the ends are less dense than those on the side surface and thereby have smaller steric hindrance,[40] leading to the formation of Au nanorods tipped by Pd nanoblocks. In the presence of 3 mM DTAB and additional Ag^+ ions, preferential deposition of PdAg nanodendrites on both ends of the DTAB-capped GNRs leads to the formation of Au nanorods tipped by PdAg nanodendrites, and the Au nanorods coated by dense PdAg nanodendrites are formed upon increasing the feeding Pd and Ag amounts. In the presence of 3 mM DTAB and 1 mM CTAB together with additional Ag^+ ions, the preferential deposition of PdAg on both ends still occurs owing to the looser capping molecules, and an arrow-shaped growth of pyramidal PdAg heads on both ends may result from a slower deposition rate in the presence of CTAB. Meanwhile, epitaxial growth of arrayed PdAg nanosheets on the four {100} lateral facets of the DTAB/CTAB-capped GNRs takes place owing to an appropriate relative ratio between the deposition rate V_{dep} and the diffusion rate V_{diff}, and the Au nanorods coated by densely packed PdAg nanosheets are formed upon increasing the concentrations of the feeding $PdCl_4^{2-}$ and Ag^+ ions. Currently, it remains unclear why the parallel PdAg nanosheet arrays show almost identical spacings between two neighboring nanosheets. It is speculated that the mixed DTAB/CTAB bilayer adsorbed on the side facets of GNRs could form separated micro-areas, namely, the DTAB-enriched micro-area and the CTAB-enriched micro-area. The initial deposition of PdAg could occur preferentially on the less strongly capped, DTAB-enriched micro-area, resulting in the formation of discrete PdAg nanosheets with a regular spacing. Nevertheless, further investigation is needed to fully elucidate the inherent growth mechanism.

The optical properties of the GNRs and the three GNR-derived heterostructures were investigated by measuring the vis-NIR absorption spectra of their dispersions in water, which is shown in Fig. 5. As expected, the GNRs with a high aspect ratio of ~7.3 exhibit a strong peak at 1097 nm corresponding to the longitudinal SPR together with a relative weak absorption peak at 510 nm corresponding to the transverse SPR, which is consistent with the reported result for the GNRs synthesized by a similar procedure.[36] For the gold nanorods tipped by Pd nanoblocks, the LSPR peak significantly diminishes and the spectrum shows a broad absorption over the whole region of 400–1300 nm instead, which may be ascribed to the plasmon damping caused by palladium coating.[30] Similarly, both the heterostructured Au/PdAg NRNDs and NRNSs show completely diminished LSPR absorption, and exhibit broad absorption over the whole region of 400–1300 nm due to the deposition of PdAg. This wide-band light absorption ability, especially for achieving full absorption in the NIR region, may endow the nano-heterostructures with great potential for efficient utilization of sunlight.[41] Particularly, the excellent absorption capacity in the visible and NIR regions lays the foundation for plasmon-enhanced catalytic activity of the heterostructured nanoparticles.

Currently, benchmark Pt-based electrocatalysts are predominantly used for the hydrogen evolution reaction (HER), but they are expensive and scarce. As an alternative, Pd-based electrocatalysts are attracting increasing interest because of the abundance, lower cost, and competitive catalytic activity of Pd.[42] Accordingly, the electrocatalytic performance of the three nano-heterostructures toward the HER was investigated by the linear sweep voltammetry test in a 0.5 M H_2SO_4 solution. Fig. 6a shows the polarization curves under dark conditions (solid lines). At a current density of 10 mA cm^{-2}, the overpotentials of Au/Pd NRNBs, Au/PdAg NRNDs, and Au/PdAg NRNSs are 0.11 V, 0.10 V and 0.08 V, respectively, indicating a sequential increase in their electrocatalytic activity with the Au/PdAg NRNSs showing the best performance. It has been recognized that alloying Pd with Ag can promote the electrocatalytic activity of Pd by modifying its electronic structure

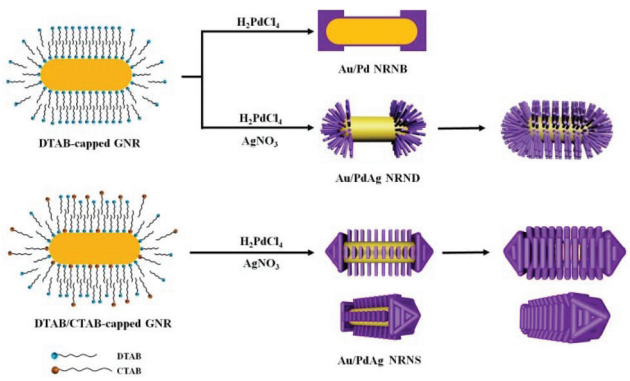

Fig. 4 Schematic illustration of the formation of Au/Pd and Au/PdAg heterostructured nanoparticles.

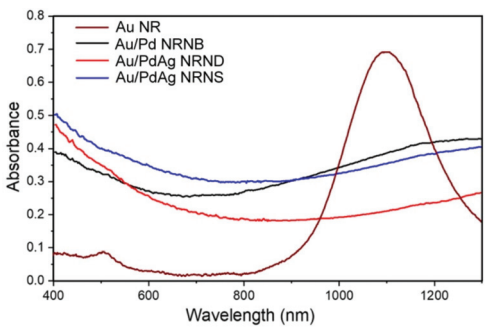

Fig. 5 Vis-NIR spectra of Au NRs, Au/Pd NRNBs, Au/PdAg NRNDs, and Au/PdAg NRNSs.

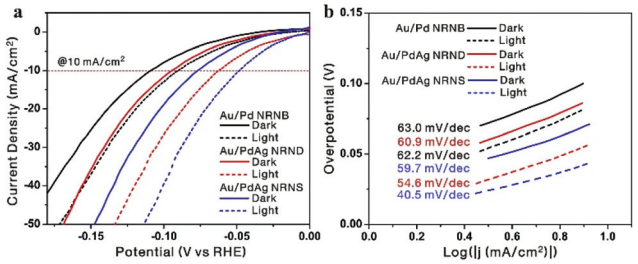

Fig. 6 HER polarization curves (a) and Tafel plots (b) of Au/Pd NRNBs, Au/PdAg NRNDs, and Au/PdAg NRNSs under dark (solid lines) and light irradiation (dashed lines) with a scan rate of 5 mV s^{-1}.

(*e.g.*, downshift of the d-band center) and forming favorable nanostructures.[21–23] Compared with the PdAg nanodendrite-tipped GNRs, the PdAg nanosheet-attached GNRs have more exposed active sites, leading to improved electrocatalytic activity. The related Tafel plots shown in Fig. 6b (solid lines) suggest that the Au/Pd NRNBs, Au/PdAg NRNDs, and Au/PdAg NRNSs exhibit Tafel slopes of 63.0, 60.9, and 59.7 mV dec^{-1}, respectively, indicating a sequential increase in both the HER kinetics and the electrocatalytic activity.

Under light illumination conditions, at a current density of 10 mA cm^{-2}, the overpotentials of the Au/Pd NRNBs, Au/PdAg NRNDs, and Au/PdAg NRNSs are considerably reduced to 0.09 V, 0.06 V, and 0.05 V respectively (Fig. 6a, dashed lines), indicating the existence of pronounced plasmon-enhanced electrocatalysis for all three nano-heterostructures. Meanwhile, the Tafel slopes of the Au/Pd NRNBs, Au/PdAg NRNDs, and Au/PdAg NRNSs are considerably decreased to 62.2, 54.6, and 40.5 mV dec^{-1}, respectively (Fig. 6b, dashed lines). These results suggest that all three hybrid nanostructures show obvious plasmon-enhanced electrocatalytic activity toward the HER with the Au/PdAg NRNDs showing the most pronounced enhancement in terms of the overpotential at 10 mA cm^{-2}, and the Au/PdAg NRNSs still exhibit the best electrocatalytic performance under light illumination. The plasmon-enhanced electrocatalytic activity may be ascribed to the hot electron transfer and the photothermal effect.[10,16,31] While the hot electron transfer can be enhanced by the local electromagnetic field enhancement, the photothermal effect can be promoted by the strong absorption in the NIR region. Therefore, the hierarchical Au/PdAg NRNSs adopt advantageous structural features for both electrocatalysis and plasmon-enhanced electrocatalysis, thus showing the best electrocatalytic and photo-assisted electrocatalytic activity.

Conclusions

Unique hierarchical Au/PdAg heterostructures consisting of regularly aligned PdAg nanosheets grown perpendicularly on Au nanorods (Au/PdAg NRNSs) were successfully synthesized in a mixed DTAB/CTAB surfactant system. The epitaxial growth of arrayed PdAg nanosheets on the four lateral {100} facets of the [100]-oriented GNRs was achieved with the assistance of the DTAB/CTAB mixture in aqueous solution. In contrast, without addition of CTAB, PdAg nanodendrite-tipped Au nanorods were produced whereas Pd nanoblock-tipped Au nanorods were obtained in the absence of Ag^{+} ions. A desirable combination of appropriate DTAB and CTAB concentrations is crucial to the formation of the unusual Au/PdAg NRNSs. At a fixed DTAB concentration, the morphology of the Au/PdAg heterostructures varies from preferential deposition of nanodendrites on both ends of the GNRs through epitaxial growth of nanosheets on the lateral facets of the GNRs to nearly conformal deposition of a thin layer with irregular protrusion on the lateral surfaces with increasing CTAB concentration. This phenomenon has been tentatively explained by considering the ratio between the deposition and diffusion rates of the PdAg alloy on the surface of gold nanorods, which are closely related to both the DTAB and CTAB concentrations. All three nano-heterostructures exhibit broad absorption over the region of 400–1300 nm, indicating potential applications in efficient utilization of solar energy. When the three nano-heterostructures were used as catalysts for the electrocatalytic hydrogen evolution reaction, the Au–PdAg NRNSs exhibited the best catalytic performance. Furthermore, all of the three heterostructures showed pronounced plasmon-enhanced catalytic activity with the Au/PdAg NRNSs exhibiting the best photo-assisted electrocatalytic activity. The hierarchical Au/PdAg NRNSs represent the first example of epitaxial 2D–1D hybrid noble metal nanostructures, and this work may open new avenues toward rational design and controllable synthesis of well-defined heterostructured nanoparticles with novel architectures and promising applications.

Conflicts of interest

There are no conflicts to declare.

Acknowledgements

This work was supported by the National Natural Science Foundation of China (Grant No. 21673007 and 21972004) and the Ministry of Science and Technology of China (2018YFA0703502).

Notes and references

1 C. Tan, J. Chen, X. J. Wu and H. Zhang, Epitaxial growth of hybrid nanostructures, *Nat. Rev. Mater.*, 2018, **3**, 17089.
2 R. Jiang, B. Li, C. Fang and J. Wang, Metal/semiconductor hybrid nanostructures for plasmon-enhanced applications, *Adv. Mater.*, 2014, **26**, 5274–5309.
3 M. Ha, J.-H. Kim, M. You, Q. Li, C. Fan and J.-M. Nam, Multicomponent plasmonic nanoparticles: from heterostructured nanoparticles to colloidal composite nanostructures, *Chem. Rev.*, 2019, **119**, 12208–12278.

4 C. Tan and H. Zhang, Epitaxial growth of heteronanostructures based on ultrathin two-dimensional nanosheets, *J. Am. Chem. Soc.*, 2015, **137**, 12162–12174.
5 H. Li, Y. Li, A. Aljarb, Y. Shi and L.-J. Li, Epitaxial growth of two-dimensional layered transition-metal dichalcogenides: growth mechanism, controllability, and scalability, *Chem. Rev.*, 2018, **118**, 6134–6150.
6 Q. Lu, A.-L. Wang, Y. Gong, W. Hao, H. Cheng, J. Chen, B. Li, N. Yang, W. Niu, J. Wang, Y. Yu, X. Zhang, Y. Chen, Z. Fan, X.-J. Wu, J. Chen, J. Luo, S. Li, L. Gu and H. Zhang, Crystal phase-based epitaxial growth of hybrid noble metal nanostructures on 4H/fcc Au nanowires, *Nat. Chem.*, 2018, **10**, 456–461.
7 J. Chen, X.-J. Wu, Y. Gong, Y. Zhu, Z. Yang, B. Li, Q. Lu, Y. Yu, S. Han, Z. Zhang, Y. Zong, Y. Han, L. Gu and H. Zhang, Edge epitaxy of two-dimensional $MoSe_2$ and MoS_2 nanosheets on one-dimensional nanowires, *J. Am. Chem. Soc.*, 2017, **139**, 8653–8660.
8 K. D. Gilroy, A. Ruditskiy, H.-C. Peng, D. Qin and Y. Xia, Bimetallic nanocrystals: syntheses, properties, and applications, *Chem. Rev.*, 2016, **116**, 10414–10472.
9 J. Gu, Y.-W. Zhang and F. Tao, Shape control of bimetallic nanocatalysts through well-designed colloidal chemistry approaches, *Chem. Soc. Rev.*, 2012, **41**, 8050–8065.
10 S. Lee, Y. W. Lee, H. Ahn, J.-H. Kim and S. W. Han, Plasmon-enhanced electrocatalysis from synergistic hybrids of noble metal nanocrystals, *Curr. Opin. Electrochem.*, 2017, **4**, 11–17.
11 S. E. Lohse and C. J. Murphy, The quest for shape control: a history of gold nanorod synthesis, *Chem. Mater.*, 2013, **25**, 1250–1261.
12 N. Li, P. Zhao and D. Astruc, Anisotropic gold nanoparticles: synthesis, properties, applications, and toxicity, *Angew. Chem., Int. Ed.*, 2014, **53**, 1756–1789.
13 J. Xiao and L. Qi, Surfactant-assisted, shape-controlled synthesis of gold nanocrystals, *Nanoscale*, 2011, **3**, 1383–1396.
14 Q. Wang, Z. Wang, Z. Li, J. Xiao, H. Shan, Z. Fang and L. Qi, Controlled growth and shape-directed self-assembly of gold nanoarrows, *Sci. Adv.*, 2017, **3**, e1701183.
15 R. Long, Y. Li, L. Song and Y. Xiong, Coupling solar energy into reactions: materials design for surface plasmon-mediated catalysis, *Small*, 2015, **11**, 3873–3889.
16 C. H. Choi, K. Chung, T.-T. H. Nguyen and D. H. Kim, Plasmon-mediated electrocatalysis for sustainable energy: from electrochemical conversion of different feedstocks to fuel cell reactions, *ACS Energy Lett.*, 2018, **3**, 1415–1433.
17 M. Dhiman, Plasmonic nanocatalysis for solar energy harvesting and sustainable chemistry, *J. Mater. Chem. A*, 2020, **8**, 10074–10095.
18 S. Li, P. Miao, Y. Zhang, J. Wu, B. Zhang, Y. Du, X. Han, J. Sun and P. Xu, Recent advances in plasmonic nanostructures for enhanced photocatalysis and electrocatalysis, *Adv. Mater.*, 2020, 2000086.
19 H.-J. Yin, J.-H. Zhou and Y.-W. Zhang, Shaping well-defined noble-metal-based nanostructures for fabricating high-performance electrocatalysts: advances and perspectives, *Inorg. Chem. Front.*, 2019, **6**, 2582–2618.
20 T. S. Rodrigues, A. G. M. da Silva and P. H. C. Camargo, Nanocatalysis by noble metal nanoparticles: controlled synthesis for the optimization and understanding of activities, *J. Mater. Chem. A*, 2019, **7**, 5857–5874.
21 W. Huang, X. Kang, C. Xu, J. Zhou, J. Deng, Y. Li and S. Cheng, 2D PdAg alloy nanodendrites for enhanced ethanol electroxidation, *Adv. Mater.*, 2018, **30**, 1706962.
22 X.-L. Xing, Y.-F. Zhao, H. Li, C.-T. Wang, Q.-X. Li and W.-B. Cai, High performance Ag rich Pd-Ag bimetallic electrocatalyst for ethylene glycol oxidation in alkaline media, *J. Electrochem. Soc.*, 2018, **165**, J3259–J3265.
23 J. Zeng, W. Zhang, Y. Yang, D. Li, X. Yu and Q. Gao, Pd–Ag alloy electrocatalysts for CO_2 reduction: composition tuning to break the scaling relationship, *ACS Appl. Mater. Interfaces*, 2019, **11**, 33074–33081.
24 Y. Zhou, R. Zhou, X. Zhu, N. Han, B. Song, T. Liu, G. Hu, Y. Li, J. Lu and Y. Li, Mesoporous PdAg nanospheres for stable electrochemical CO_2 reduction to formate, *Adv. Mater.*, 2020, 2000992.
25 H. Chen, L. Shao, Q. Li and J. Wang, Gold nanorods and their plasmonic properties, *Chem. Soc. Rev.*, 2013, **42**, 2679–2724.
26 S. F. Tan, G. Bisht, U. Anand, M. Bosman, X. E. Yong and U. Mirsaidov, In situ kinetic and thermodynamic growth control of Au–Pd core–shell nanoparticles, *J. Am. Chem. Soc.*, 2018, **140**, 11680–11685.
27 H. Huang, L. Zhang, Z. Lv, R. Long, C. Zhang, Y. Lin, K. Wei, C. Wang, L. Chen, Z.-Y. Li, Q. Zhang, Y. Luo and Y. Xiong, Unraveling surface plasmon decay in core–shell nanostructures toward broadband light-driven catalytic organic synthesis, *J. Am. Chem. Soc.*, 2016, **138**, 6822–6828.
28 Y. Huang, A. R. Ferhan, A. Dandapat, C. S. Yoon, J. E. Song, E. C. Cho and D. H. Kim, A strategy for the formation of gold–palladium supra-nanoparticles from gold nanoparticles of various shapes and their application to high-performance H_2O_2 sensing, *J. Phys. Chem. C*, 2015, **119**, 26164–26170.
29 J. Guo, Y. Zhang, L. Shi, Y. Zhu, M. F. Mideksa, K. Hou, W. Zhao, D. Wang, M. Zhao, X. Zhang, J. Lv, J. Zhang, X. Wang and Z. Tang, Boosting hot electrons in hetero-superstructures for plasmon-enhanced catalysis, *J. Am. Chem. Soc.*, 2017, **139**, 17964–17972.
30 G. Su, H. Jiang, H. Zhu, J.-J. Lv, G. Yang, B. Yan and J.-J. Zhu, Controlled deposition of palladium nanodendrites on the tips of gold nanorods and their enhanced catalytic activity, *Nanoscale*, 2017, **9**, 12494–12502.
31 Y. Wei, Z. Zhao and P. Yang, Pd-tipped Au nanorods for plasmon-enhanced electrocatalytic hydrogen evolution with photoelectric and photothermal effects, *ChemElectroChem*, 2018, **5**, 778–784.
32 M. Tsuji, K. Takemura, C. Shiraishi, K. Ikedo, K. Uto, A. Yajima, M. Hattori, Y. Nakashima, K. Fukutomi, K. Tsuruda, T. Daio, T. Tsuji and S. Hata, Syntheses of Au@PdAg and Au@PdAg@Ag core–shell nanorods through

distortion-induced alloying between Pd shells and Ag atoms over Au nanorods, *J. Phys. Chem. C*, 2015, **119**, 10811–10823.

33 Q. Zhang, X. Guo, Z. Liang, J. Zeng, J. Yang and S. Liao, Hybrid PdAg alloy–Au nanorods: controlled growth, optical properties and electrochemical catalysis, *Nano Res.*, 2013, **6**, 571–580.

34 H. Zhang, Z. Liu, X. Kang, J. Guo, W. Ma and S. Cheng, Asymmetric AgPd–AuNR heterostructure with enhanced photothermal performance and SERS activity, *Nanoscale*, 2016, **8**, 2242–2248.

35 C. Fang, G. Zhao, Z. Zhang, J. Zheng, Q. Ding, X. Xu, L. Shao and B. Geng, Morphology engineering of Au/(PdAg alloy) nanostructures for enhanced electrocatalytic ethanol oxidation, *Part. Part. Syst. Charact.*, 2018, **35**, 1800258.

36 L. Vigderman and E. R. Zubarev, High-yield synthesis of gold nanorods with longitudinal SPR peak greater than 1200 nm using hydroquinone as a reducing agent, *Chem. Mater.*, 2013, **25**, 1450–1457.

37 Q. Wang, D. Li, J. Xiao, F. Guo and L. Qi, Reversible self-assembly of gold nanorods mediated by photo-switchable molecular adsorption, *Nano Res.*, 2019, **12**, 1563–1569.

38 M. Li, Z. Ge, S. Zhang, P. He, Y. Gu, L. Qi and Y. Shao, Electrocatalytic reduction of hydrogen peroxide by Pd-Ag nanoparticles based on the collisional approach, *ChemElectroChem*, 2018, **5**, 3021–3027.

39 Y. Xia, K. D. Gilroy, H.-C. Peng and X. Xia, Seed-mediated growth of colloidal metal nanocrystals, *Angew. Chem., Int. Ed.*, 2017, **56**, 60–95.

40 H. Jia, A. Du, H. Zhang, J. Yang, R. Jiang, J. Wang and C.-y. Zhang, Site-selective growth of crystalline ceria with oxygen vacancies on gold nanocrystals for near-infrared nitrogen photofixation, *J. Am. Chem. Soc.*, 2019, **141**, 5083–5086.

41 D. Liu, F. Zhou, C. Li, T. Zhang, H. Zhang, W. Cai and Y. Li, Black gold: plasmonic colloidosomes with broadband absorption self-assembled from monodispersed gold nanospheres by using a reverse emulsion system, *Angew. Chem., Int. Ed.*, 2015, **54**, 9596–9600.

42 A. Chen and C. Ostrom, Palladium-based nanomaterials: synthesis and electrochemical applications, *Chem. Rev.*, 2015, **115**, 11999–12044.